QSAR Modeling and Molecular Docking Studies of 3,5-Disubstituted Indole Derivatives as Pim1 Inhibitors for Combating Hematological Cancer

Y. EL Allouche[a],*, H. Zaitan[a], M. Bouachrine[b] and F. Khalil[a]

[a]*Laboratory of Processes, Materials, and Environment (LPME), Faculty of Science and Technology, Sidi Mohamed Ben Abdellah University, Fez, Morocco*
[b]*MCNS Laboratory, Faculty of Sciences, Moulay Ismail University, Meknes, Morocco*

Cancer has become a global health concern, with escalating mortality rates in the 21st century, leading the World Health Organization to recognize it as one of the deadliest diseases. In their search for new anticancer therapeutic agents, researchers have identified the 3,5-disubstituted Indole derivatives as potential therapeutic agents capable of targeting the Proviral integration of moloney (Pim) kinases that correlate to hematological cancers. This study aims to investigate a series of 3,5-disubstituted indole derivatives as potent inhibitors of Pim1 kinase. Different computational chemistry techniques were utilized, including 2D-QSAR and molecular docking, to design novel inhibitors for targeting Pim1. The analysis of 2D-QSAR results showed that the inhibitory activity might be predicted with high accuracy ($R^2_{test} = 0.96$) using a classical statistical modeling technique, namely partial least squares regression. The six inhibitors that were identified as highly bio-active, were subjected to the docking study, and the results highlighted the important Pi-Alkyl interactions rising between the ligands and the Pim-1 kinase receptor (PDB code: 5DWR), which may enhance the binding of the ligand to a hydrophobic pocket on the target receptor. Overall, the combination of 2D-QSAR, molecular docking, and ADMET analysis has provided valuable insights and potential avenues for further exploration in the development of effective hematological anticancer agents.

Keywords: 3.5-Disubstituted Indole derivatives, QSAR, Docking, Pim1, Anticancer

INTRODUCTION

According to the World Health Organization estimates, cancer is the primary or second major cause of death before the age of 70 in 112 of 183 nations. It accounts for approximately one in six global fatalities [1]. Hematological cancer, in particular, has emerged as a significant target for research and therapeutic development in this context [2,3]. Hematological malignancies, along with solid tumors, often activate the Pim kinases, a family of serine/threonine kinases encompassing Pim-1, Pim-2, and Pim-3. These enzymes play pivotal roles in regulating diverse signaling pathways associated with cancer initiation and progression [4]. Notably, despite variations in their expression levels and distinct

functions, compelling evidence supports the involvement of all three Pim genes in cancer through a compensatory mechanism [5]. Consequently, extensive research efforts, both in academic and pharmaceutical sectors, have focused on the development of Pim kinase inhibitors, aligning with the prevailing trend in oncology, which emphasizes kinase inhibition as a prominent therapeutic approach [6,7]. Among these inhibitors, the Pim1 inhibitor stands out due to its unique biochemical and molecular characteristics, which influence various oncogenic pathways [8]. Its ability to impede cancer cell proliferation, migration, and growth has positioned it as a promising therapeutic agent, often employed in combination with other chemotherapy components [9,10]. Indoles, recognized for their intrinsic anticancer properties, have garnered significant attention for their capacity to mitigate cell death in specific cancer types [11]. These naturally occurring bioactive compounds, found in various sources, exhibit

───────────
*Corresponding author. E-mail: Yassine.elallouche@usmba.ac.ma

diverse biochemical activities, underscoring their importance in biomedical research and drug discovery [12]. The field of hematological anticancer therapy faces an urgent need for the discovery of novel treatments [13]. To address this need, our study conducted an in-depth analysis of 32 constituents comprising 3,5-disubstituted indole derivatives, utilizing the 2D-QSAR (2D-Quantitative Structure-Activity Relationship) methodology. This rigorous analysis yielded valuable insights that can guide the development of novel compounds with potent hematological anticancer properties. In parallel with the 2D-QSAR analysis [14], we employed molecular docking techniques to investigate the molecular-level interactions between selected ligands and the Pim-1 kinase receptor (PDB code: 5DWR). Our aim was to gain deeper insights into how these compounds interact with the target receptor and potentially inhibit its activity. Building upon the insights derived from the 2D-QSAR analysis and molecular docking investigations [15], we utilized in-silico methods to design four innovative compounds. These compounds were carefully constructed by incorporating features and structural elements derived from the 2D-QSAR analyses, with the aim of optimizing their interactions with the Pim-1 kinase receptor and enhancing their hematological anticancer activity. This in-silico design of new compounds represents an innovative approach toward the development of potential candidates for hematological anticancer therapy [16]. By leveraging computational methodologies and insights from 2D-QSAR analyses and molecular docking studies, our goal is to expedite the discovery of novel compounds with improved efficacy and reduced side effects. Further experimental validation and optimization of these compounds are warranted to confirm their potential as promising candidates in the treatment of hematological cancers.

MATERIALS AND METHODS

Data Collection

We acquired a database of 32 compounds from previously published work [12]. This database encompasses various 3,5-disubstituted indole derivatives that have been identified as inhibitors of Pim kinase. The database was randomly partitioned into two distinct sets; 26 compounds were used as training set for QSAR models' development, and the remaining 6 compounds were used as testing set for models

testing. Table 1 furnishes a comprehensive summary of the distinct molecular structures present in both the training and test sets, along with their corresponding biological activities, quantified as pIC50 values.

ChemDraw was used to draw the molecular structures, while Chem3D provided the tools for optimization and energy minimization. To optimize and stabilize them, we used the Molecular Mechanics 2 (MM2) force field [17]. This approach enabled us to source the most favorable geometries for the molecules studied. By combining these two software packages, we were able to obtain reliable and accurate molecular models for our study.

2D QSAR Studies

Molecular Operating Environment (MOE) is used to compute 206 2D-descriptors; For simplicity, descriptors that had a weak link to activity were disregarded. In the QSAR analysis, the most pertinent descriptors were chosen and employed as independent variables [18,19].

PLS Analysis

The Partial Least Squares (PLS) method is commonly employed to examine the linear relationship between the target variable and independent variables [20,21,22]. PLS analysis enables the determination of key factors contributing to the potency of these inhibitors. Several parameters are assessed during the PLS analysis [23], including the cross-validation coefficient of determination (Q^2), the coefficient of determination (R^2), the number of components (N), and the Root Mean Square Error (RMSE). The selection of the best QSAR model is based on high R^2 and Q^2 values, indicating a strong correlation between the independent variables and the target variable [24,25]. To evaluate the robustness of the models generated, external validation was performed using the testing set comprising six molecules.
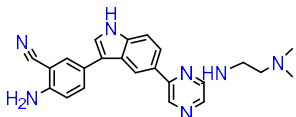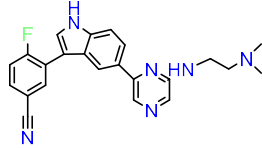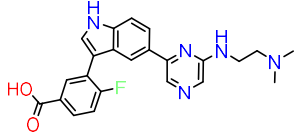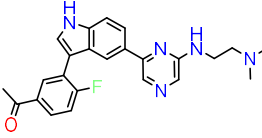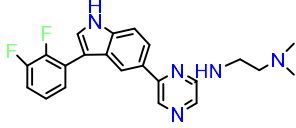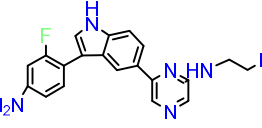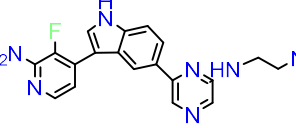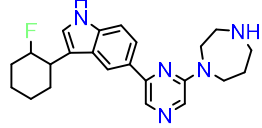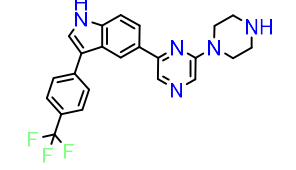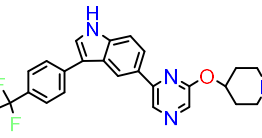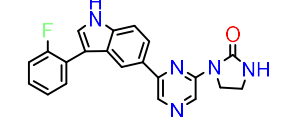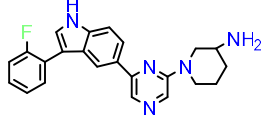
Molecular Docking

The protein kinase Pim-1, with the PDB ID 5DWR, was obtained from the Protein Data Bank (www.rcsb.org) for our study. The focus of our research was to investigate the binding interactions between Pim-1 protein kinase and various ligands. For the molecular docking studies [26,27], Autodock Tools [28] was employed. To prepare the proteins, the receptor (Pim-1 protein kinase) underwent hydrogen addition

Table 1. Chemical Structures and their Related Activity Values (* Test Set Compounds)

N°	Structure of compound	pIC50	N°	Structure of compound	pIC50
L1*		7.72	L2		7.68
L3		7.17	L4		7.46
L5		8.10	L6		7.72
L7		7.48	L8*		7.68
L9		8.05	L10		8.15
L11		7.02	L12		6.87
L13		7.66	L14*		7.52
L15		8.15	L16		6.80
L17		7.68	L18		8.05
L19*		6.84	L20*		6.59

Table 1. Continued

L21		8.30	L22		8.05
L23		7.64	L24		8.52
L25*		8.05	L26		8.52
L27		8.52	L28		6.92
L29		6.59	L30		6.73
L31		6.59	L32		8.15

and removal of water molecules as part of the docking protocol [29]. Autodock Vina [30] was utilized to carry out these steps for both the receptor and the ligands. To analyze the results obtained from the molecular docking studies, we employed Discovery Studio 2016 (www.discover.3ds.com) and pymol (WWW.pymol.org) software. These tools provided us with the necessary capabilities to analyze and interpret the outcomes of the docking experiments.

Prediction of Pharmacokinetic Properties

It is crucial to consider the pharmacological activity of compounds and optimize their ADMET (Absorption, Distribution, Metabolism, Excretion, and Toxicity) profiles to enhance the success of potential drug discovery or research tools. *In-silico* analysis can address the criteria and ADMET characteristics of candidate drugs, which have been assessed

using accessible online servers such as pkCSM [31].

RESULTS AND DISCUSSION

2D-QSAR Modeling Results

A predictive 2D-QSAR model, presented by Eq. (1), was developed using the PLS method. Its performance was evaluated and summarized in Table 2. Three descriptors, namely *balabanJ*, *PEOE_RPC+*, and SMR_*VSA4* were included in the model.

pIC50 = 1.75453 + 4.46441*(balabanJ) - 5.65542*(PEOE_RPC+) + 0.02138*(SMR_VSA4) (1)

The PLS equation, derived from the given data set, played a crucial role in this process. It encapsulated the mathematical

Table 2. Summary of QSAR Model Performance

N	R^2	RMSE	Q^2	R^2_{test}	cRp^2
25	0.81	0.26	0.71	0.96	0.76

representation of the linear model and served as a tool for prediction and analysis [32]. By incorporating the PLS equation, researchers were able to investigate the influence of various independent variables on the dependent variable. This approach was selected due to its effectiveness in handling multicollinearity [33], a common issue in QSAR modeling, where independent variables are highly correlated. PLS addressed this challenge by constructing latent variables, which are linear combinations of the original variables that capture the maximum variance in the data [34]. By utilizing the PLS equation, the investigators aimed to gain insights into the quantitative relationship between the independent variables and the dependent variable. This allowed for the identification of important features or descriptors that contributed significantly to the model's predictive power (Table 3). Additionally, the PLS equation facilitated the assessment of the model's performance and provided a means to make predictions for new data points based on the learned relationships.

Model's Validation

To assess the predictive accuracy of the 2D-QSAR models developed using the training set, we made predictions on the biological activities of six molecules in an external testing set (Table 4). The reliability and performance of the models were evaluated using the determination coefficient of external validation (R^2_{test}) [35].

To ensure the stability of the constructed QSAR model,

Y-randomization [36] was carried out. This method involves validating the model by randomly shuffling the response parameters (Y) while keeping the descriptors (X) unchanged. parameter called cRp^2 should be greater than 0.5 as per the equation (Eq. (2)):

$$cRp^2 = R*(R^2 - (\text{Average } R)^2)^{1/2} \qquad (2)$$

Interpretation of the 2D-QSAR Descriptors

The coefficients of the molecular descriptors in Eq. (1) suggest that the 2D descriptor, specifically the coefficient of the Balaban topological index (*BalabanJ*) [37], represents the relative positive partial charge (*PEOE_RPC+*) [38]. Additionally, the descriptor (*SMR_VSA4*) [39] represents the sum of the van der Waals surface where Ri (molar refractivity for atom (i)) falls within the range of 0.39 and 0.44. These descriptors have the most significant influence on the inhibitory potency of Pim1 kinase of 3,5-disubstituted indoles.

The positive coefficients of the two topological descriptors, *BalabanJ* and *SMR_VSA4*, indicate that an increase in these descriptors corresponds to an increase in the inhibitory potency of Pim1 kinase of 3,5-disubstituted indoles. On the other hand, the topological coefficient of *PEOE_RPC+* is negative, suggesting that a decrease in *PEOE_RPC+* leads to an increase in the inhibitory potency of Pim1 kinase of 3,5-disubstituted indoles.

Newly Designed Compounds

Based on the findings of the 2D QSAR analysis and the recommendations derived from the selected descriptors, the presence of an eight-membered ring can indeed exert an influence on topological indices. Moreover, the presence of such an eight-membered ring within a molecule can give rise

Table 3. Correlation Matrix for the Two Selected Descriptors

Variables	balabanJ	PEOE_RPC+	SMR_VSA4	pIC50
balabanJ	1.000	-0.222	0.356	0.680
PEOE_RPC+	-0.222	1.000	-0.259	-0.682
SMR_VSA4	0.356	-0.259	1.000	0.572
pIC50	0.680	-0.682	0.572	1.000

Table 4. Descriptors, Observed, Predicted, and Residual Values

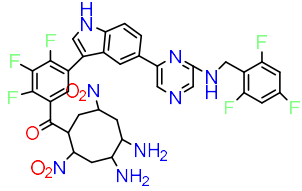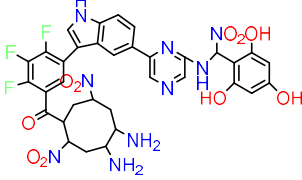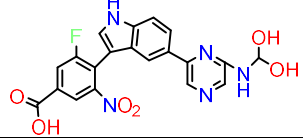| N°	BalabanJ	PEOE_RPC+	SMR_VSA4	pIC50	Pred(pIC50)	Residual
			Training set			
L2	1.311372	0.08638086	37.36924	7.6800	7.9196	-0.2396
L3	1.293102	0.18118526	37.36924	7.1700	7.3019	-0.1319
L4	1.328322	0.18115045	37.36924	7.4600	7.4593	0.0007
L5	1.300344	0.07894928	40.12599	8.1000	7.9714	0.1286
L6	1.311372	0.07892931	40.12599	7.7200	8.0207	-0.3007
L7	1.292163	0.08334168	37.36924	7.4800	7.8510	-0.3710
L9	1.292046	0.07824656	37.36924	8.0500	7.8793	0.1707
L10	1.312062	0.07822695	37.36924	8.1500	7.9688	0.1812
L11	1.272579	0.21599703	37.36924	7.0200	7.0134	0.0066
L12	1.311786	0.21595043	37.36924	6.8700	7.1887	-0.3187
L13	1.300344	0.08437382	37.36924	7.6600	7.8817	-0.2217
L15	1.323407	0.08324916	37.36924	8.1500	7.9911	0.1589
L16	1.113315	0.07720553	43.7404	6.8000	7.2235	-0.4235
L17	1.293102	0.09198904	37.36924	7.6800	7.8063	-0.1263
L18	1.293102	0.11978569	68.66068	8.0500	8.3183	-0.2683
L21	1.319127	0.07446075	40.12599	8.3000	8.0806	0.2194
L22	1.33839	0.07949366	37.36924	8.0500	8.0792	-0.0292
L23	1.34647	0.11717431	37.36924	7.6400	7.9022	-0.2622
L24	1.34647	0.07525036	37.36924	8.5200	8.1393	0.3807
L26	1.324659	0.07541274	40.12599	8.5200	8.0999	0.4201
L27	1.335602	0.07133184	39.69717	8.5200	8.1627	0.3573
L28	1.214127	0.08220991	12.98734	6.9200	6.9877	-0.0677
L29	1.176297	0.18397638	19.35849	6.5900	6.3795	0.2105
L30	1.148456	0.17706668	17.03057	6.7300	6.2445	0.4855
L31	1.233576	0.14512503	19.35849	6.5900	6.8549	-0.2649
L32	1.216565	0.08111265	52.25568	8.1500	7.8445	0.3055
			Test set			
L1	1.300344	0.08638013	37.36924	7.7200	7.8595	-0.1395
L8	1.312203	0.08331887	37.36924	7.6800	7.9274	-0.2474
L14	1.311372	0.08435101	37.36924	7.5200	7.9184	-0.3984
L19	1.342531	0.17373851	37.36924	6.8400	7.5868	-0.7468
L20	1.317602	0.1737318	37.36924	6.5900	7.4779	-0.8879
L25	1.335602	0.07829792	37.36924	8.0500	8.0559	-0.0059
			Prediction			
P1	1.1291928	0.050266538	103.16362	N/A	8.717069	N/A
P2	1.1501068	0.045478839	103.16362	N/A	8.837515	N/A
P3	1.4516307	0.090163	40.125992	N/A	8.583189	N/A

to regions of uneven electron density. Consequently, disparities in the partial charges of atoms located within the ring in comparison to those positioned outside of it become apparent. In instances where the eight-membered ring incorporates oxygen or nitrogen atoms, these atoms tend to exhibit higher electronegativity, thus leading to the manifestation of negative partial charges. This differential distribution of charges can subsequently be reflected in the relative positive partial charge values observed among specific atoms within the molecule. Furthermore, within the realm of medicinal chemistry and the domain of drug design, the presence of an eight-membered ring within a molecule can wield a substantial influence over its interactions with specific biological targets. Molecular interactions, particularly those related to protein binding, may undergo modulation due to the structural characteristics associated with eight-membered rings and the relative partial charges of atoms located within these ring structures. Similarly, for alcohol and nitro groups, three compounds, specifically denoted as P1, P2, and P3, have been proposed considering this analysis. Notably, these compounds exhibited a marked enhancement in inhibitory activity along with significantly higher overall scores when compared to the most potent compounds in the dataset. The corresponding pIC50 values for these compounds, along with their respective molecular structures, are presented in Table 5.

Docking Results

Molecular docking analyses were conducted on a set of six compounds, consisting of three highly active molecules (L24, L26, and L27) and three predicted molecules (P1, P2, and P3), utilizing the AutoDock Vina software [30]. Prior to the docking simulation, the receptor was prepared by eliminating all water molecules and heteroatoms. The aim of the docking simulation was to assess the binding energy between the ligands and the receptor, as well as to investigate the binding positions of the ligands. The obtained results demonstrated binding affinity values of -10.3, -9.7, -9.5, -12.7, -11.3, and -8.7 kcal mol^{-1} for the designed molecules L24, L26, L27, P1, P2, and P3, respectively. These findings provide substantial evidence for the stability of the proposed three molecules.

Protein-ligand interactions were further investigated using Discovery Studio software for the target protein (PDB ID: 5DWR) and the compounds L24, L26, L27, P1, P2, and P3. The details of these interactions are presented in Table 6, and

Table 5. Chemical Structures and their Predicted Activity

N°	Structure of compound	Pred(pIC50)
P1		8.71
P2		8.83
P3		8.58

a graphical representation can be found in Figs. 1,2,3,4, 5 and 6.

Compound L24 (Fig. 1) exhibited seven Pi-Alkyl bonds with residues Lys67, Val52, Ile185, Leu120, Ile104, Leu174, and Ala65. Additionally, a Conventional Hydrogen Bond was observed at a distance of 2.07 Å with the Asp128 residue. Furthermore, at a distance of 3.77 Å, the benzene ring of L24 engaged in Carbon Hydrogen Bond interactions with Asn172, Pi-Pi Stacked interactions with Phe49, and Unfavorable Acceptor-Acceptor interactions with Lys67.

Similarly, compound L26 (Fig. 2) displayed the same interactions as L24, except for Conventional Hydrogen Bonds occurring with Glu121 and Asp128 at distances of 2.63 Å and 1.80 Å, respectively.

Compound L27 (Fig. 3) displayed significant interactions, including seven Pi-Alkyl bonds with residues Lys67, Val52, Leu120, Ile185, Ile104, Pro123, and Arg122. Moreover, distinct Pi-Sigma interactions were observed with Val52, Ile185, and Leu174 at distances of 3.88 Å, 3.93 Å, and 3.63 Å, respectively. Additionally, Pi-Pi Stacked interactions were identified with Phe49, while Unfavorable Acceptor-Acceptor interactions were observed with Lys67. These interactions contribute to the molecular recognition and

Table 6. Pim1 Interaction Residues with L24, L26, L27, P1, P2 and P3

N°	Concentional hydrogen bond	Carbon hydrogen bond	Halogen (Fluorine)	Pi-Alkyl	Pi-Anion	Pi-Cation	Pi-Sigma	Pi-Pi Stacked	Pi-Pi T-Shaped	Unfavorable acceptor-acceptor
L24	Asp128	Asn172		Lys67. Val52. Ile185. Leu120. Ile104. Leu174. Ala65				Phe49		Lys67
L26	Glu121 Asp128	Asn172		Lys67. Val52. Ile185. Leu120. Ala65. Leu174. Ile104				Phe49		Lys67
L27				Lys67. Val52. Leu120. Ile185. Ala65. Ile104. Pro123. Arg122			Val52. Ile185. Leu174	Phe49		Lys67
P1	Asn172. Asp128. Asp131	Glu171	Gly48. Asp167. Asp186. Glu121	Lys67. Ile185. Val52. Ala65. Leu174		Lys169			Phe49	Lys67
P2	Val126. Asp131. Leu44. Ser46	Arg122 Asn172	Glu121	Lys67. Ile186. Ala6. Leu174. Val52	Asp128		Val52	Phe49		Asp131
P3	Asp128	Asp186. Asp172. Glu171. Gly45		Leu44. Val52	Asp128		Ile185. Val52	Phe49		
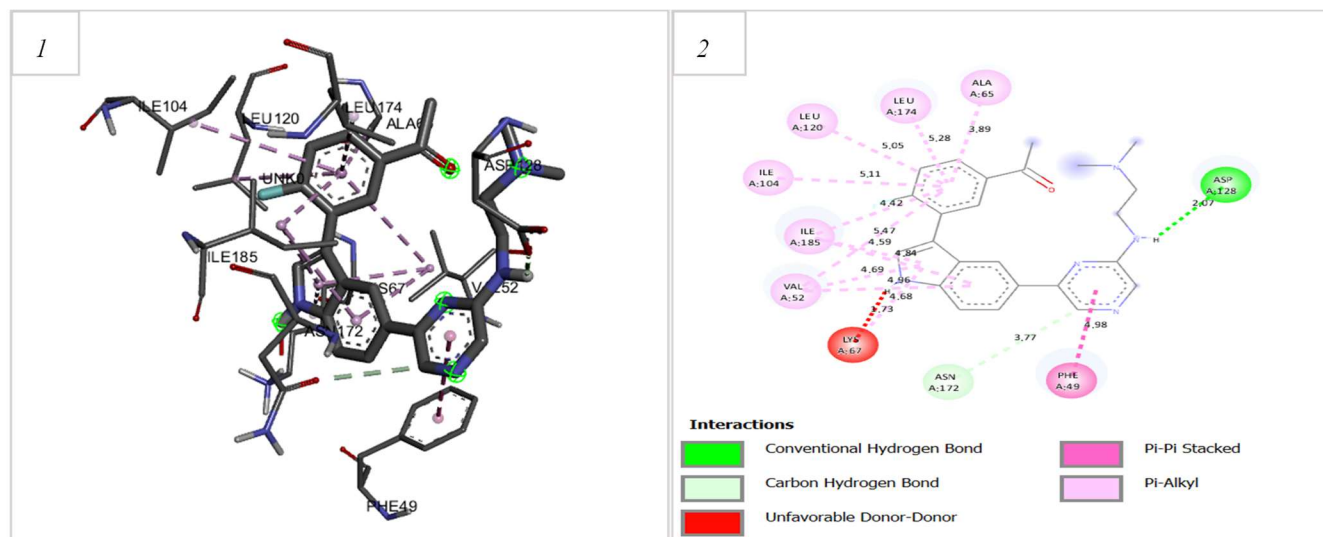
Fig. 1. Analysis of the anchoring of compound L24 in the binding pocket of the pim-1 receptor kinase. (1) 3D interactions of the ligand-receptor complex, (2) 2D interactions of the ligand-receptor complex (residues).
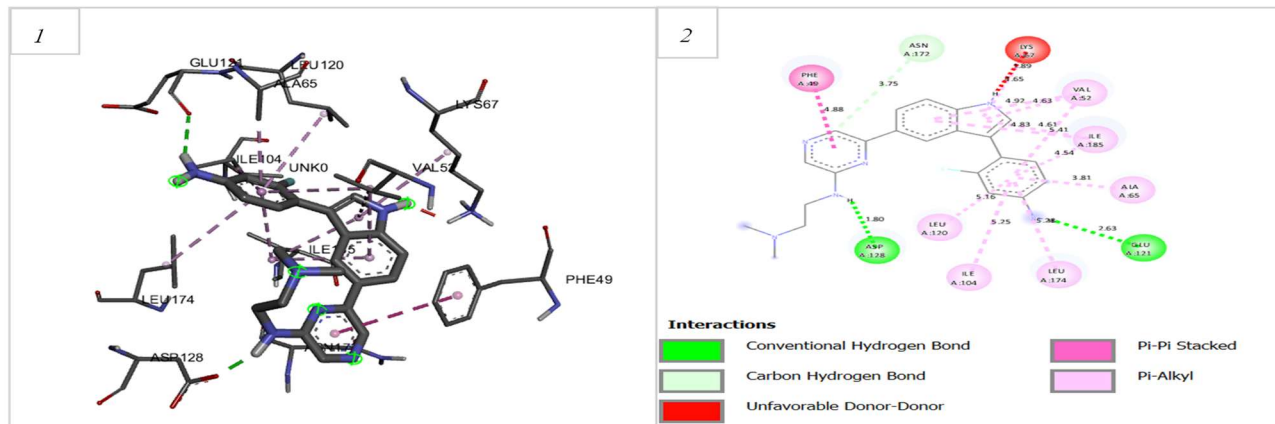
Fig. 2. Analysis of the anchoring of compound L26 in the binding pocket of the pim-1 receptor kinase. (1) 3D interactions of the ligand-receptor complex, (2) 2D interactions of the ligand-receptor complex (residues).

Fig. 3. Analysis of the anchoring of compound L27 in the binding pocket of the pim-1 receptor kinase. (1) 3D interactions of the ligand-receptor complex, (2) 2D interactions of the ligand-receptor complex (residues).
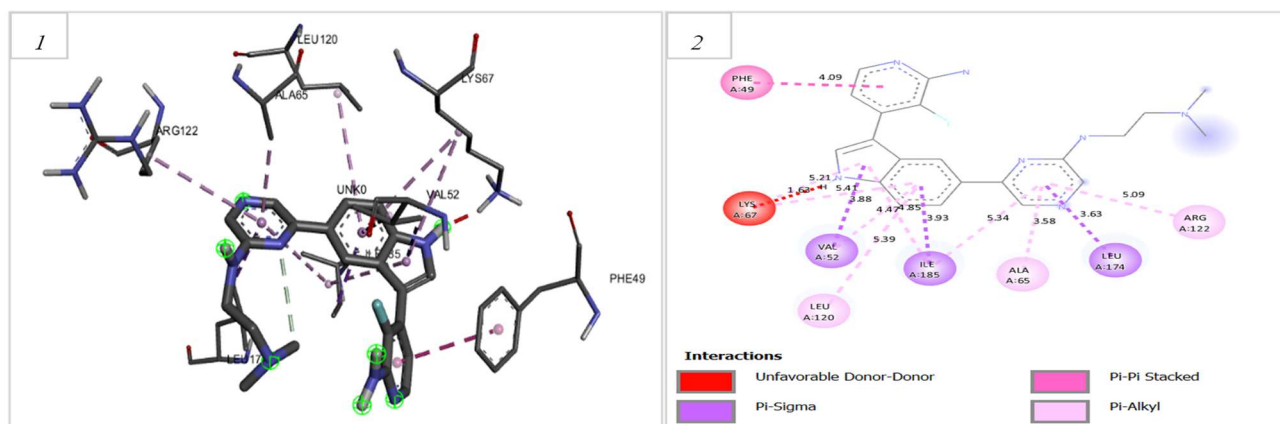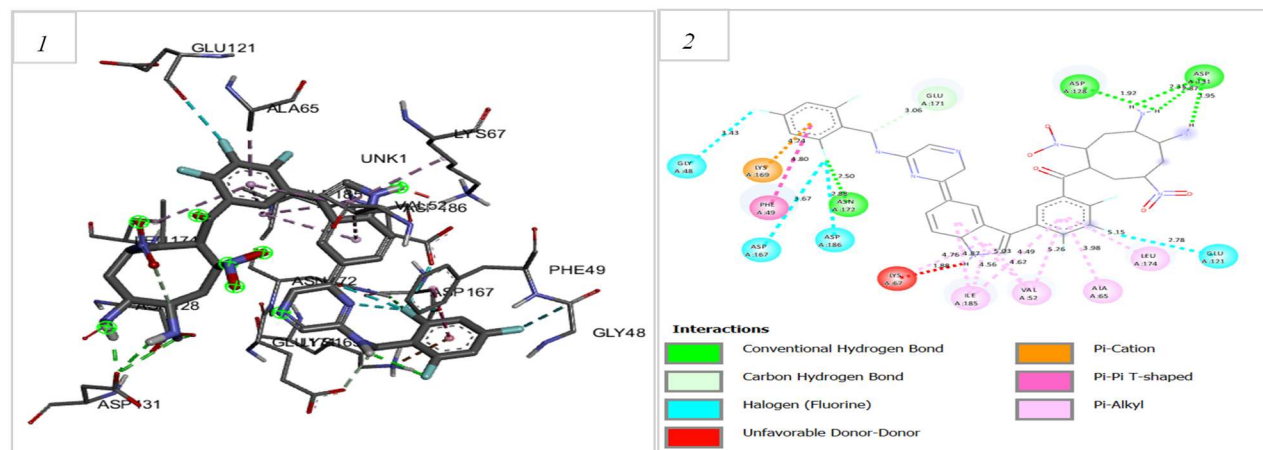

Fig. 4. Analysis of the anchoring of compound P1 in the binding pocket of the pim-1 receptor kinase. (1) 3D interactions of the ligand-receptor complex, (2) 2D interactions of the ligand-receptor complex (residues).

Fig. 5 . Analysis of the anchoring of compound P2 in the binding pocket of the pim-1 receptor kinase. (1) 3D interactions of the ligand-receptor complex, (2) 2D interactions of the ligand-receptor complex (residues).

Fig. 6. Analysis of the anchoring of compound P3 in the binding pocket of the pim-1 receptor kinase. (1) 3D interactions of the ligand-receptor complex, (2) 2D interactions of the ligand-receptor complex (residues).
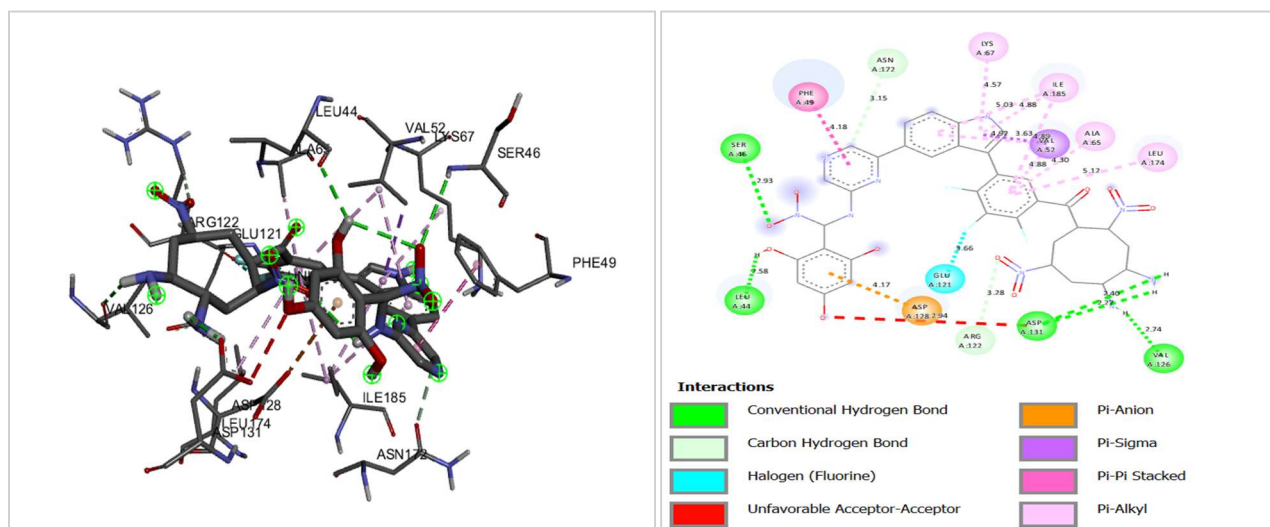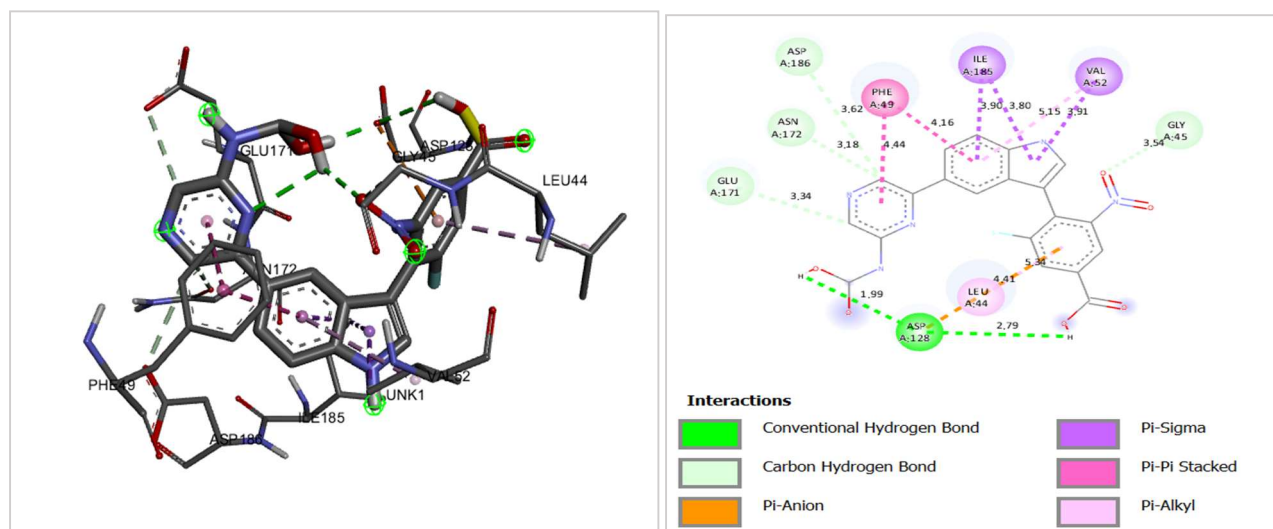
binding of compound L27 with the target protein.

Compound P1 (Fig. 4) showed a highly favorable binding capacity. The optimized conformational energy of the ligand is attributed to several key interactions. These include Pi-alkyl interactions with Lys67, Val52, Ile185, Ala65, and Leu174, respectively. Additionally, Halogen (Fluorine) interactions occurred with Gly48, Asp167, Asp186, and Glu121 at distances of 3.43 Å, 3.67 Å, 2.88 Å, and 2.78 Å, respectively. Furthermore, Conventional Hydrogen Bonds were formed with Asn172, Asp128, and Asp131, respectively. Other interactions observed include Carbon Hydrogen Bond interactions with Glu171, Pi-Cation interactions with Lys169,

Pi-Pi T-Shaped interactions with Phe49, and Unfavorable Acceptor-Acceptor interactions with Lys67.

Similarly, compound P2 (Fig. 5) showed strong binding to the target site (5DWR) through Pi-alkyl interactions with Lys67, Ile186, Ala65, Leu174, and Val52, respectively. Additionally, Conventional Hydrogen Bond interactions occurred with Val126, Asp131, Leu44, and Ser46, respectively. Further interactions were observed at distances of 3.28 Å and 3.15 Å between the compound P2 and Arg122 and Asn172, respectively, via Carbon Hydrogen Bonds. Furthermore, Halogen (Fluorine) interactions occurred with Glu121, Pi-Anion interactions with Asp128, Pi-Sigma interactions with Val52, Pi-Pi Stacked interactions with Phe49, and Unfavorable Acceptor-Acceptor interactions with Asp131. These interactions contributed significantly to the binding affinity and stability of compound P2 with the target protein.

In addition, compound P3 (Fig. 6) displayed notable interactions with the target protein. It formed two Carbon Hydrogen Bonds and two hydrogen bonds between the OH group and the residue Asp128. Additionally, P3 established a four Carbon Hydrogen Bond network with residues Asp186, Asp172, Glu171, and Gly45. Pi-Alkyl interactions were observed between P3 and residues Leu44 and Val52. Moreover, P3 formed Pi-Alkyl interactions with Asp128, Pi-Sigma interactions with Ile185 and Val52, and Pi-Pi Stacked interactions with Phe49. These interactions contributed to the binding and stability of compound P3 within the target protein.

ADMET Predictions

Pharmacokinetic and toxicity assessments were conducted through ADMET (Absorption. Distribution. Metabolism. Excretion. and Toxicity) analysis and the PKCSM web server. A summarized presentation of the results is provided in Table 7. The limitation in a drug's bioavailability and its biological effects is intricately linked to its absorption capacity. Notably. the designed products exhibited extensive absorption potential. as evidenced by their human intestinal absorption (HIA) values exceeding 30%. Furthermore, the evaluation of these substances included an assessment of their inhibitory or substrate activity concerning cytochrome P450 enzymes, which served as an additional indicator of their metabolic fate. Cytochrome P450 enzymes play a pivotal role in the elimination of exogenous organic molecules, including pharmaceuticals, and are indispensable for the oxidation processes within the body. It is noteworthy that all ligands examined were identified as substrates of 3A4 with the exceptions being L26 and P3, which exhibited no interaction with 2D6. Additionally, the results derived from inhibition studies indicated that none of the molecules displayed inhibitory effects on 2D6. Moreover, the outcomes of toxicity assessments, encompassing AMES toxicity evaluations, affirm the non-toxic nature of the predicted chemicals [40]. It is imperative to consider that chemicals with a Log PS value exceeding -2 are deemed capable of permeating the central nervous system (CNS), whereas compounds with a Log PS value below -3 may encounter challenges in crossing the CNS barrier. Additionally, the concept of drug clearance involves comparing the rate at which a drug is eliminated from the body to its rate of presence. Interestingly, none of the newly designed ligands exhibited issues related to drug persistence. In summary, the comprehensive pharmacokinetic and toxicity evaluations conducted through ADMET analysis and the PKCSM web server underscored the favorable characteristics of the designed compounds, including their high absorption potential, metabolic compatibility, and non-toxic nature. These findings bode well for their future development and potential application as pharmaceutical agents.

CONCLUSION

In this study, we examined an extensive investigation into a series of thirty-two 3.5-disubstituted indole derivatives with the aim of identifying potent inhibitors of Pim1 kinase, employing the 2D-QSAR technique as our primary analytical tool. Our rigorous analysis yielded highly promising statistical results, reflecting a remarkable level of reliability and exceptional predictive capability. The insights gleaned from our comprehensive 2D-QSAR studies furnished valuable information concerning the essential structural features that are crucial for both favorable and unfavorable substitutions influencing inhibitory activity. Building upon these insights, we took a proactive step by proposing novel 3.5-disubstituted indole derivatives. These proposed compounds were meticulously designed based on the descriptors employed in our study, with the goal of optimizing their interaction with the Pim1 receptor kinase. To delve deeper into the nature of

Table 7. ADMET Prediction of the Template (L24. L26. and L27) in the Data Set and Novel Inhibitors

Ligand	Absorption	Distribution		Metabolism							Excretion	Toxicity
				CYP								
				Substrate		Inhibitor						
	Intestinal absorption	VDss	CNS	2D6	3A4	1A2	2C19	2C9	2D6	3A4	Total clearance	AMES toxicity
	Numeric (% Absorbed)	Numeric (log l/kg)	Numeric (logPS)			Categorical (yes/no)					Numeric (log (ml/min/kg))	Categorical (yes/no)
L24	94.363	1.072	-2.393	No	Yes	Yes	Yes	Yes	No	Yes	0.686	No
L26	92.394	0.663	-1.166	No	No	Yes	Yes	No	No	Yes	0.706	Yes
L27	80.79	1.269	-2.7	No	Yes	Yes	Yes	Yes	No	Yes	0.777	Yes
P1	77.284	-0.696	-3.623	No	Yes	No	No	No	No	Yes	-0.484	No
P2	60.143	-0.458	-4.103	No	Yes	No	No	No	No	No	-0.746	No
P3	44.54	-1.559	-3.53	No	No	No	No	No	No	No	0.229	No

these interactions, molecular docking studies were rigorously conducted using Autodock. It is worth noting that our proposed compounds exhibited a level of stability that surpassed that of previously reported compounds in the literature, representing a significant stride in our research. Equally paramount in our investigation was ensuring the safety profile of these proposed compounds. To this end, we conducted AMES Toxicity Analysis, and the results were reassuring. All three of the proposed compounds successfully passed the toxicity assessment, bolstering our confidence in their potential for further development and clinical exploration. As we navigate the path forward, it is essential to underscore the importance of synthesizing these compounds in the laboratory. Experimental validation will not only verify their efficacy but also provide critical data on their safety profile. By synthesizing and rigorously testing these novel derivatives, we aim to gain a deeper and more comprehensive understanding of their potential as hematological anticancer agents. In conclusion, this research represents a significant stride in the quest for novel hematological anticancer therapies.

The amalgamation of advanced computational techniques, molecular design, and toxicity assessment underscores the holistic approach employed in this study. As we stand at the precipice of laboratory synthesis and subsequent experimental validation, we hold the promise of contributing to the advancement of therapies aimed at combatting hematological cancers, potentially improving the prognosis and quality of life for affected individuals.

REFERENCES

[1] Sung, H.; Ferlay, J.; Siegel, R. L.; Laversanne, M.; Soerjomataram, I.; Jemal, A.; Bray, F., Global Cancer Statistics 2020: GLOBOCAN Estimates of Incidence and Mortality Worldwide for 36 Cancers in 185 Countries. *CA: A Cancer J. Clin.* **2021**, *71* (3), 209-249. DOI: 10.3322/caac.21660.

[2] Clements, A. N.; Warfel, N. A., Targeting PIM Kinases to Improve the Efficacy of Immunotherapy. *Cells* **2022**, *11* (22), 3700. DOI:10.3390/cells11223700.

[3] García-Suárez, J.; de la Cruz, J.; Cedillo, Á.; Llamas, P.; Duarte, R.; Jiménez-Yuste, V.; Hernández-Rivas, J. Á.; Gil-Manso, R.; Kwon, M.; Sánchez-Godoy, P.; Martínez-Barranco, P.; Colás-Lahuerta, B.; Herrera, P.; Benito-Parra, L.; Alegre, A.; Velasco, A.; Matilla, A.; Aláez-Usón, M. C.; Martos-Martínez, R.; Martínez-Chamorro, C.; Susana-Quiroz, K.; Del Campo, J. F.; de la Fuente, A.; Herráez, R.; Pascual, A.; Gómez, E.; Pérez-Oteyza, J.; Ruiz, E.; Alonso, A.; González-Medina, J.; Martín-Buitrago, L. N.; Canales, M.; González-Gascón, I.; Vicente-Ayuso, M. C.; Valenciano, S.; Roa, M. G.; Monteliu, P. E.; López-Jiménez, J.; Escobar, C. E.; Ortiz-Martín, J.; Diez-Martin, J. L.; Martinez-Lopez, J.; Serí-Merino, C.; Queiroz-Cervantes, K.; Fernandez, M. E.; Peñalva-Moreno, M.-J.; Naya-Errea, D.; Bermejo-Martínez, L.; Llorente-González, L., the Asociación Madrileña de Hematología y Hemoterapia (AMHH). Impact of Hematologic Malignancy and Type of Cancer Therapy on COVID-19 Severity and Mortality: Lessons from a Large Population-Based Registry Study. *J. Hematol. Oncol.* **2020**, *13* (1), 133. DOI: 10.1186/s13045-020-00970-7.

[4] Rathi, A.; Kumar, D.; Hasan, G. M.; Haque, M. M.; Hassan, M. I., Therapeutic Targeting of PIM KINASE Signaling in Cancer Therapy: Structural and Clinical Prospects. *Biochim. Biophys. Acta Gen. Subj.* **2021**, *1865* (11), 129995. DOI: 10.1016/j.bbagen.2021.129995.

[5] Wu, J.; Chu, E.; Kang, Y., PIM Kinases in Multiple Myeloma. *Cancers* **2021**, *13* (17), 4304. DOI: 10.3390/cancers13174304.

[6] Roskoski, R., Properties of FDA-Approved Small Molecule Protein Kinase Inhibitors: A 2020 Update. *Pharmacol. Res.* **2020**, *152*, 104609. DOI: 10.1016/j.phrs.2019.104609.

[7] Attwood, M. M.; Fabbro, D.; Sokolov, A. V.; Knapp, S.; Schiöth, H. B., Trends in Kinase Drug Discovery: Targets, Indications and Inhibitor Design. *Nat. Rev. Drug Discov.* **2021**, *20* (11), 839-861. DOI: 10.1038/s41573-021-00252-y.

[8] Borchardt, H.; Ewe, A.; Morawski, M.; Weirauch, U.; Aigner, A., miR24-3p Activity after Delivery into Pancreatic Carcinoma Cell Lines Exerts Profound

[9] Tumor-Inhibitory Effects through Distinct Pathways of Apoptosis and Autophagy Induction. *Cancer Lett.* **2021**, *503*, 174-184. DOI: 10.1016/j.canlet.2021.01.018.

[10] Zhao, G.; Ren, Y.; Yan, J.; Zhang, T.; Lu, P.; Lei, J.; Rao, H.; Kang, X.; Cao, Z.; Peng, F.; Peng, C.; Rao, C.; Li, Y., Neoprzewaquinone A Inhibits Breast Cancer Cell Migration and Promotes Smooth Muscle Relaxation by Targeting PIM1 to Block ROCK2/STAT3 Pathway. *IJMS* **2023**, *24* (6), 5464. DOI: 10.3390/ijms24065464.

[11] Yi, X.; Cao, Z.; Yuan, Y.; Li, W.; Cui, X.; Chen, Z.; Hu, X.; Yu, A., Design and Synthesis of a Novel Mitochondria-Targeted Osteosarcoma Theranostic Agent Based on a PIM1 Kinase Inhibitor. *J. Controlled Release* **2021**, *332*, 434-447. DOI: 10.1016/j.jconrel.2021.02.028.

[12] Qin, R.; You, F.-M.; Zhao, Q.; Xie, X.; Peng, C.; Zhan, G.; Han, B., Naturally Derived Indole Alkaloids Targeting Regulated Cell Death (RCD) for Cancer Therapy: From Molecular Mechanisms to Potential Therapeutic Targets. *J. Hematol. Oncol.* **2022**, *15* (1), 133. DOI:10.1186/s13045-022-01350-z.

[13] More, K. N.; Hong, V. S.; Lee, A.; Park, J.; Kim, S.; Lee, J., Discovery and Evaluation of 3,5-Disubstituted Indole Derivatives as Pim Kinase Inhibitors. *Bioorg. Med. Chem. Lett.* **2018**, *28* (14), 2513-2517. DOI: 10.1016/j.bmcl.2018.05.054.

[14] Podhorecka, M., Metformin - Its Anti-Cancer Effects in Hematologic Malignancies. *Oncol. Rev.,* **2021**, *15* (1), 514. DOI: 10.4081/oncol.2021.514.

[15] Elmchichi, L.; Belhassan, A.; Aouidate, A.; Ghaleb, A.; Lakhlifi, T.; Bouachrine, M., QSAR Study of New Compounds Based on 1,2,4-Triazole as Potential Anticancer Agents. *PCR* **2020**, *8* (1). DOI: 10.22036/pcr.2019.204753.1685.

[16] Bouachrine, M.; Elmchichi, L.; El Aissouq, A.; Belhassan, A.; Zaki, H.; Ouammou, A.; Lakhlifi, T., Molecular Docking, Drug Likeness Studies and ADMET Prediction of Flavonoids as Platelet-Activating Factor (PAF) Receptor Binding. *Chem. Rev. Lett.* **2021**, *4* (3). DOI: 10.22034/crl.2021.262806.1098.

[17] El Rhabori, S.; El Aissouq, A.; Chtita, S.; Khalil, F., Design of Novel Quinoline Derivatives as Antibreast Cancer Using 3D-QSAR, Molecular Docking and Pharmacokinetic Investigation. *Anti-Cancer Drugs* **2022**, *33* (9), 789-802. DOI: 10.1097/ CAD.0000000000001318.

[18] El Aissouq, A.; Bouachrine, M.; Ouammou, A.; Khalil, F., Homology Modeling, Virtual Screening, Molecular Docking, Molecular Dynamic (MD) Simulation, and ADMET Approaches for Identification of Natural Anti-Parkinson Agents Targeting MAO-B Protein. *Neurosci. Lett.* **2022**, *786*, 136803. DOI: 10.1016/ j.neulet.2022.136803.

[19] ElMchichi, L.; Belhassan, A.; Lakhlifi, T.; Bouachrine, M. 3D-QSAR Study of the Chalcone Derivatives as Anticancer Agents. *J. Chem.* **2020**, *2020*, 1-12. DOI: 10.1155/2020/5268985.

[20] Aissouq, A. E.; Lachhab, A.; Rhabori, S. E.; Bouachrine, M.; Ouammou, A.; Khalil, F., Computer-Aided Drug Design Applied to a Series of Pyridinyl Imidazole Derivatives Targeting P38α MAP Kinase: 2D-QSAR, Docking, MD Simulation, and ADMET Investigations. *New J. Chem.* **2022**, *46* (43), 20786-20800. DOI: 10.1039/D2NJ03686J.

[21] Aissouq, A. E.; Bouachrine, M.; Ouammou, A.; Khalil, F., Computational Investigation of Unsaturated Ketone Derivatives as MAO-B Inhibitors by Using QSAR, ADME/Tox, Molecular Docking, and Molecular Dynamics Simulations. *Turk. J. Chem.* **2022**, *46* (3), 687-703. DOI: 10.55730/1300-0527.3360.

[22] Abderrahim, D.; Taoufiq, S.; Bouchaib, I.; Rabie, R., Enhancing Tomato Leaf Nitrogen Analysis through Portable NIR Spectrometers Combined with Machine Learning and Chemometrics. *Chemometrics and Intelligent Laboratory Systems* **2023**, *240*, 104925. DOI: 10.1016/j.chemolab.2023.104925.

[23] Diane, A.; Saffaj, T.; Ihssane, B.; Rabie, R., The Synergic Approach between Machine Learning, Chemometrics, and NIR Hyperspectral Imagery for a Real-Time, Reliable, and Accurate Prediction of Mass Loss in Cement Samples. *Heliyon* **2023**, *9* (5), e15898. DOI: 10.1016/j.heliyon.2023.e15898.

[24] Mali, S. N.; Pandey, A., Multiple QSAR and Molecular Modelling for Identification of Potent Human Adenovirus Inhibitors. *J. Ind. Chem. Soc.* **2021**, *98* (6), 100082. DOI: 10.1016/j.jics.2021.100082.

[25] Mali, S. N.; Pandey, A.; Bhandare, R. R.; Shaik, A. B., Identification of Hydantoin Based Decaprenyl-phosphoryl-β-d-Ribose Oxidase (DprE1) Inhibitors as Antimycobacterial Agents Using Computational Tools. *Sci. Rep.* **2022**, *12* (1), 16368. DOI: 10.1038/s41598-022-20325-1.

[26] Laoud, A.; Aliracedi, F.; Ferkous, F., Discovery of New Inhibitors of Enoyl-ACP Reductase via Structure-Based Virtual Screening. *Phys. Chem. Res.* **2023**, *11* (3), 459-469. DOI: 10.22036/ pcr.2022.342259.2106.

[27] Ghosh, S.; Mali, S. N.; Bhowmick, D. N.; Pratap, A. P., Neem Oil as Natural Pesticide: Pseudo Ternary Diagram and Computational Study. *J. Ind. Chem. Soc.* **2021**, *98* (7), 100088. DOI: 10.1016/j.jics.2021.100088.

[28] Mali, S. N.; Pandey, A., Synthesis of New Hydrazones Using a Biodegradable Catalyst, Their Biological Evaluations and Molecular Modeling Studies (Part-II). *J. Comput. Biophys. Chem.* **2022**, *21* (07), 857-882. DOI: 10.1142/S2737416522500387.

[29] Morris, G. M.; Huey, R.; Lindstrom, W.; Sanner, M. F.; Belew, R. K.; Goodsell, D. S.; Olson, A. J., AutoDock4 and AutoDockTools4: Automated Docking with Selective Receptor Flexibility. *J. Comput. Chem.* **2009**, *30* (16), 2785-2791. DOI:10.1002/jcc.21256.

[30] Laoud, A.; Ferkous, F.; Maccari, L.; Maccari, G.; Saihi, Y.; Kraim, K., Identification of Novel Nt-MGAM Inhibitors for Potential Treatment of Type 2 Diabetes: Virtual Screening, Atom Based 3D-QSAR Model, Docking Analysis and ADME Study. *Comput. Biol. Chem.* **2018**, *72*, 122-135. DOI: 10.1016/ j.compbiolchem.2017.12.003.

[31] Trott, O.; Olson, A. J., AutoDock Vina: Improving the Speed and Accuracy of Docking with a New Scoring Function, Efficient Optimization and Multithreading. *J. Comput. Chem.* **2010**, *31* (2), 455-461. DOI: 10.1002/ jcc.21334.

[32] Pires, D. E. V.; Blundell, T. L.; Ascher, D. B., pkCSM: Predicting Small-Molecule Pharmacokinetic and

Toxicity Properties Using Graph-Based Signatures. *J. Med. Chem.* **2015**, *58* (9), 4066-4072. DOI: 10.1021/ acs.jmedchem.5b00104.

[33] Sihvonen, T.; Duma, Z. -S.; Haario, H.; Reinikainen, S. -P., Spectral Profile Partial Least-Squares (SP-PLS): Local Multivariate Pansharpening on Spectral Profiles. *ISPRS Open Journal of Photogrammetry and Remote Sensing* **2023**, *10*, 100049. DOI: 10.1016/ j.ophoto.2023.100049.

[34] Sadiq, M., Modeling Survival Response Using a Parametric Approach in the Presence of Multicollinearity. *Communications in Statistic-Simulation and Computation* **2022**, 1-10. DOI: 10.1080/ 03610918.2022.2060509.

[35] Kumar, K. Partial Least Square (PLS) Analysis. *Reson* **2021**, *26* (3), 429-442. DOI: 10.1007/s12045-021-1140-1.

[36] El Rhabori, S.; El Aissouq, A.; Chtita, S.; Khalil, F., QSAR, Molecular Docking and ADMET Studies of Quinoline, Isoquinoline and Quinazoline Derivatives against Plasmodium Falciparum Malaria. *Struct. Chem.* **2023**, *34* (2), 585-603. DOI: 10.1007/s11224-022-01988-y.

[37] Chatterjee, M.; Roy, K., Application of Cross-Validation Strategies to Avoid Overestimation of Performance of 2D-QSAR Models for the Prediction of Aquatic Toxicity of Chemical Mixtures. *SAR and QSAR in Environmental Research* **2022**, *33* (6), 463-484. DOI: 10.1080/1062936X.2022.2081255.

[37] Bennani, F. E.; Doudach, L.; Karrouchi, K.; El rhayam, Y.; Rudd, C. E.; Ansar, M.; El Abbes Faouzi, M., Design and Prediction of Novel Pyrazole Derivatives as Potential Anti-Cancer Compounds Based on 2D-QSAR Study against PC-3, B16F10, K562, MDA-MB-231, A2780, ACHN and NUGC Cancer Cell Lines. *Heliyon* **2022**, *8* (8), e10003. DOI: 10.1016/ j.heliyon.2022.e10003.

[38] Andini, S.; Araya-Cloutier, C.; Lay, B.; Vreeke, G.; Hageman, J.; Vincken, J. -P., QSAR-Based Physicochemical Properties of Isothiocyanate Antimicrobials against Gram-Negative and Gram-Positive Bacteria. *LWT* **2021**, *144*, 111222. DOI: 10.1016/j.lwt.2021.111222.

[39] Abd El-Meguid, E. A.; Naglah, A. M.; Moustafa, G. O.; Awad, H. M.; El Kerdawy, A. M., Novel Benzothiazole-Based Dual VEGFR-2/EGFR Inhibitors Targeting Breast and Liver Cancers: Synthesis, Cytotoxic Activity, QSAR and Molecular Docking Studies. *Bioorg. Med. Chem. Lett.* **2022**, *58*, 128529. DOI: 10.1016/j.bmcl.2022.128529.

[40] Laddha, A. P.; Murugesan, S.; Kulkarni, Y. A., *In-Vivo* and in-Silico Toxicity Studies of Daidzein: An Isoflavone from Soy. *Drug Chem. Toxicol.* **2022**, *45* (3), 1408-1416. DOI: 10.1080/ 01480545.2020.1833906.